

Systematic Investigation on Morphologies, Forming Mechanism, Photocatalytic and Photoluminescent Properties of ZnO Nanostructures Constructed in Ionic Liquids

Li Wang,^{†,‡} Lixian Chang,[†] Bin Zhao,^{*,†} Zhongyong Yuan,[†] Gaosong Shao,[†] and Wenjun Zheng^{*,†}

College of Chemistry, Nankai University, Tianjin 300071, P. R. China, and Chemistry Department, Xinjiang Normal University, Urumqi 830054, P. R. China

Received June 4, 2007

In this contribution, a series of shape-controllable ZnO nanostructures were synthesized in ionic liquids by a simpler, only one-step, low-temperature route, and characterized by XRD, XPS, TEM, HRTEM, SAED, EDXA, SEM, FTIR, surface area measurement and photoluminescence. We mainly investigate the effect of cations of ionic liquids on the shape of ZnO nanostructures and the forming mechanism of ZnO nanostructures in ionic liquids, as well as the luminescent property and photocatalytic activity for the degradation of Rhodamine B. The results show that the longer alkyl chain at position-1 of the imidazole ring of the ionic liquid will hinder the ZnO nanostructures from growing longer, and the hydrogen bonds may play a crucial role for the directional growth of the 1D nanocrystals. The photoluminescent study shows that the as-obtained ZnO nanostructures exhibit a unique green emission, indicating the existence of oxygen vacancies in the ZnO nanostructures. Importantly, the as-obtained ZnO nanostructures prepared in different ionic liquids show strong size/shape-dependent photocatalysis activity for degradation of Rhodamine B, and the well-dispersed homogeneous ZnO nanoparticles and nanowires display high photocatalytic activity. The investigation of photodegradation kinetics of Rhodamine B indicates that the photodegradation process obeys the rule of a first-order kinetic equation $\ln(C_0/C) = kt$. This is the first systematic investigation on the relationship between the structure of ionic liquids and the morphology of ZnO nanostructures.

Introduction

Zinc oxide, as a wide band gap semiconductor oxide with a large excitation binding energy (60 meV), becomes one of the most important electronic and photonic materials. Although research on ZnO nanostructures has come through many decades, the renewed interest is inspired by the availability of high-quality materials with new properties, and great progress has been made, which was witnessed by many excellent papers.^{1–22} For instance, in 2001, Yang et

al. observed the room-temperature UV-lasing generated from 1D ZnO nanomaterials.^{1,2} In 2006, Wang et al. reported that nanoscale mechanical energy was converted into electrical energy by means of piezoelectric zinc oxide nanowire arrays,

* To whom correspondence should be addressed. E-mail: zhaobin@nankai.edu.cn (B.Z.), zhwj@nankai.edu.cn (W.Z.).

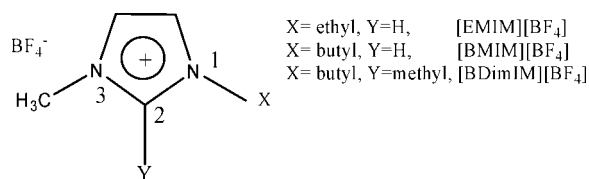
[†] Nankai University.

[‡] Xinjiang Normal University.

- (1) Huang, M. H.; Mao, S.; Feick, H. N.; Yan, H. Q.; Wu, Y. Y.; Kind, H.; Weber, E.; Russo, R.; Yang, P. D. *Science* **2001**, *292*, 1897.
- (2) Yang, P.; Yan, H.; Mao, S.; Russo, R.; Johnson, J.; Saykally, R.; Morris, N.; Pham, J.; He, R.; Choi, H.-J. *Adv. Funct. Mater.* **2002**, *12*, 323.
- (3) Wang, Z. L.; Song, J. H. *Science* **2006**, *312*, 242.
- (4) Wang, X. D.; Song, J. H.; Liu, J.; Wang, Z. L. *Science* **2007**, *316*, 102.
- (5) Liu, B.; Zeng, H. C. *J. Am. Chem. Soc.* **2004**, *126*, 16744.

- (6) Liu, B.; Zeng, H. C. *J. Am. Chem. Soc.* **2003**, *125*, 4430.
- (7) Andelman, T.; Gong, Y. Y.; Polking, M.; Yin, M.; Kuskovsky, I.; Neumark, G.; O'Brien, S. *J. Phys. Chem. B* **2005**, *109*, 14314.
- (8) Cheng, B.; Shi, W. S.; Russell-Tanner, J. M.; Zhang, L.; Samulski, E. T. *Inorg. Chem.* **2006**, *45*, 1208.
- (9) Cheng, B.; Samulski, E. T. *Chem. Commun.* **2004**, 986.
- (10) Yin, M.; Gu, Y.; Kuskovsky, I. L.; Andelman, T.; Zhu, Y. M.; Neumark, G. F.; O'Brien, S. *J. Am. Chem. Soc.* **2004**, *126*, 6206.
- (11) Zhu, Z. M.; Chen, T. L.; Gu, Y.; Warren, J.; Osgood, R. M., Jr. *Chem. Mater.* **2005**, *17*, 4227.
- (12) Kong, Y. C.; Yu, D. P.; Zhang, B.; Fang, W.; Feng, S. Q. *Appl. Phys. Lett.* **2001**, *78*, 407.
- (13) Zheng, M. J.; Zhang, L. D.; Li, G. H.; Shen, W. Z. *Chem. Phys. Lett.* **2002**, *363*, 123.
- (14) Zhang, J.; Sun, L. D.; Pan, H. Y.; Liao, C. S.; Yan, C. H. *New J. Chem.* **2002**, *26*, 33.
- (15) Li, Z. Q.; Xiong, Y. J.; Xie, Y. *Inorg. Chem.* **2003**, *42*, 8105.
- (16) Hu, Y.; Chen, J.; Xue, X.; Li, T. W.; Xie, Y. *Inorg. Chem.* **2005**, *44*, 7280.
- (17) Gao, X. P.; Zheng, Z. F.; Zhu, H. Y.; Pan, G. L.; Bao, J. L.; Wu, F.; Song, D. Y. *Chem. Commun.* **2004**, 1428.

Scheme 1. Chemical Structures of Ionic Liquids



and then, they continued to report a nanowire nanogenerator that is driven by an ultrasonic wave to produce continuous direct-current output in 2007.^{3,4}

Recently, ionic liquids, a new class of solvents with ionic character, have been widely employed in organic reactions and electrochemical devices, because of their negligible vapor pressure, high ionic conductivity, and a large electrochemical window.^{23–25} However, in contrast to successful applications in organic and electrochemistry, the use of ionic liquids in inorganic synthesis is still in its infancy. Most recently, the advantages of ionic liquids in inorganic synthesis have been gradually realized; a few inorganic materials, such as mesoporous silica²⁶ and supermicroporous silica,²⁷ iridium²⁸ and gold²⁹ nanoparticles, TiO₂ nanocrystals³⁰ and microspheres,³¹ Te³² and CoPt³³ nanorods, and so on,^{34–37} have been fabricated in ionic liquids. However, to our best of knowledge, systematic investigations on the relationship between the structures of ionic liquids and the morphology of ZnO nanostructures have no report hitherto. More importantly, the formation mechanisms of ZnO nanostructures in these three ionic liquids (Scheme 1) have not been investigated in detail.

As a developing method, the low-temperature solid-state route has been successfully applied to the synthesis of a series of nanomaterials, showing specific advantages.³⁸ Inspired by

this, we wonder whether the ionic liquids would affect the morphology of the final product if the ionic liquids were introduced into a low-temperature solid-state reaction, because when an ionic liquid is used as a reaction solvent, the solute is solvated by ions, thus, the reaction proceeds in an environment totally different from that when water or ordinary organic solvents are used, and therefore, a novel morphology could be expected.

With this kind of curiosity, by introducing three kinds of imidazolium ionic liquids (Scheme 1) into the low-temperature solid-state reaction, we mainly explored the effect of cations of ionic liquids on the shape of ZnO nanostructures, and the forming mechanism of ZnO nanostructures in ionic liquids, as well as luminescent property and photocatalytic activity for the degradation of Rhodamine B. The experimental results showed that hydrogen bonds, formed between the hydrogen atom at position-2 of the imidazole ring and the oxygen atoms of O–Zn crystal cores, may act as an effective bridge to connect the produced nuclei of zinc oxide and cations of ionic liquids, playing a crucial role for the 1D nanocrystals' directional growing. Furthermore, a longer alkyl chain at position 1 of the imidazole ring of the ionic liquid will hinder the 1D ZnO nanostructures from growing longer because of the steric hindrance effect. The photoluminescent results show that the as-obtained ZnO nanostructures exhibit unique green emission property, suggesting the existence of oxygen vacancies in the ZnO nanostructures. More importantly, the as-obtained ZnO nanostructures in different ionic liquids show a strong size/shape-dependence of the photocatalysis activity for degradation of Rhodamine B, and the well-dispersed homogeneous ZnO nanostructures display high photocatalytic activity. The kinetics of photodegradation of Rhodamine B is also studied. $\ln(C_0/C)$ is linear with the irradiation time, indicating that photodegradation of Rhodamine B obeys the rule of a first-order kinetic reaction $\ln(C_0/C) = kt$, and the apparent rate constant k is also calculated. To our knowledge, this is the first systematic investigation on the relationship between the structure of ionic liquids and the morphology of ZnO nanostructures.

Experimental Section

Synthesis of sample 1 (ZnO nanoparticles): All of the reagents employed were commercially available and used as received without further purification. Typically, 4.0 mmol Zn(CH₃COO)₂·2H₂O were ground for about 20 min in agate mortar, followed by the addition of 2 mL ionic liquid [EMIM][BF₄] (1-ethyl-3-methylimidazolium tetrafluoroborate, Scheme 1) and 8.0 mmol sodium hydroxide fine powder. The mixture was ground for 30 min and heated at 80 °C for 48 h to ensure the completeness of reaction. Then, it was dried in the air after being washed by alcohol and water.

The syntheses of samples 2–10 were identical with that of sample 1 except that the ionic liquids, the amount of sodium hydroxide, and the reaction temperature were different. The detailed synthesis

- (18) Xu, L. F.; Guo, Y.; Liao, Q.; Zhang, J. P.; Xu, D. S. *J. Phys. Chem. B* **2005**, *109*, 13519.
 (19) Li, W. J.; Shi, E. W.; Chen, Z. Z.; Yin, Z. W. *Chin. Sci. Bull.* **2000**, *45*, 1662.
 (20) Vanheusden, K.; Warren, W. L.; Seager, C. H.; Tallant, D. R.; Voigt, J. A.; Gnade, B. E. *J. Appl. Phys.* **1996**, *79*, 7983.
 (21) Huang, M. H.; Wu, Y. Y.; Feick, H. N.; Tran, N.; Weber, E.; Yang, P. D. *Adv. Mater.* **2001**, *13*, 113.
 (22) Zhang, J.; Sun, L. D.; Yin, J. L.; Su, H. L.; Liao, C. S.; Yan, C. H. *Chem. Mater.* **2002**, *14*, 4172.
 (23) Welton, T. *Chem. Rev.* **1999**, *99*, 2071.
 (24) Kumar, A. *Chem. Rev.* **2001**, *101*, 1.
 (25) Wasserscheid, P.; Keim, W. *Angew. Chem., Int. Ed.* **2000**, *39*, 3772.
 (26) Zhou, Y.; Schattka, J. H.; Antonietti, M. *Nano Lett.* **2004**, *4*, 477.
 (27) Zhou, Y.; Antonietti, M. *Chem. Mater.* **2004**, *16*, 544.
 (28) Dupont, J.; Fonseca, G. S.; Umpierre, A. P.; Fichtner, P. F. P.; Teixeira, S. R. *J. Am. Chem. Soc.* **2002**, *124*, 4228.
 (29) Itoh, H.; Naka, K.; Chujo, Y. *J. Am. Chem. Soc.* **2004**, *126*, 3026.
 (30) Zhou, Y.; Antonietti, M. *J. Am. Chem. Soc.* **2003**, *125*, 14960.
 (31) Nakashima, T.; Kimizuka, N. *J. Am. Chem. Soc.* **2003**, *125*, 6386.
 (32) Zhu, Y. J.; Wang, W. W.; Qi, R. J.; Hu, X. L. *Angew. Chem., Int. Ed.* **2004**, *43*, 1410.
 (33) Wang, Y.; Yang, H. *J. Am. Chem. Soc.* **2005**, *127*, 5316.
 (34) (a) Deshmukh, R. R.; Rajagopal, R.; Srinivasan, K. V. *Chem. Commun.* **2000**, 1544. (b) Zhu, J. M.; Shen, Y. H.; Xie, A. J.; Qiu, L. G.; Zhang, Q.; Zhang, S. Y. *J. Phys. Chem. C* **2007**, *111*, 7629. (c) Park, H.; Yang, S. H.; Jun, Y. S.; Hong, W. H.; Kang, J. K. *Chem. Mater.* **2007**, *19*, 535. (d) Biswas, K.; Rao, C. N. R. *Chem.—Eur. J.* **2007**, *13*, 6123. (e) Yu, N. Y.; Gong, L. M.; Song, H. J.; Liu, Y.; Yin, D. H. *J. Solid State Chem.* **2007**, *180*, 799. (f) Bhatt, A. I.; Mechler, A.; Martin, L. L.; Bond, A. M. *J. Mater. Chem.* **2007**, *17*, 2241.
 (35) Zhou, X.; Xie, Z. X.; Jiang, Z. Y.; Kuang, Q.; Zhang, S. H.; Xu, T.; Huang, R. B.; Zheng, L. S. *Chem. Commun.* **2005**, 5572.
 (36) Wang, L.; Zhao, B.; Yuan, Z. Y.; Zhang, X. J.; Wu, Q. D.; Chang, L. X.; Zheng, W. J. *Sci. China, Ser. B* **2007**, *50*, 63.

- (37) (a) Wang, W. W.; Zhu, Y. J. *Inorg. Chem. Commun.* **2004**, *7*, 1003. (b) Wang, J.; Cao, J. M.; Fang, B. Q.; Lu, P.; Deng, S. G.; Wang, H. Y. *Mater. Lett.* **2005**, *59*, 1405. (c) Hou, X. M.; Zhou, F.; Sun, Y. B.; Liu, W. M. *Mater. Lett.* **2007**, *61*, 1789. (d) Wang, L.; Zhao, B.; Chang, L. X.; Zheng, W. J. *Sci. China, Ser. B* **2007**, *50*, 224.
 (38) (a) Wang, R. Y.; Jia, D. Z.; Zhang, L.; Liu, L.; Guo, Z. P.; Li, B. Q.; Wang, J. X. *Adv. Funct. Mater.* **2007**, *16*, 687. (b) Ye, X. R.; Jia, D. Z.; Yu, J. Q.; Xin, X. Q.; Xue, Z. L. *Adv. Mater.* **1999**, *11*, 941.

Table 1. ZnO Samples with Different Morphologies Prepared in Three Kinds of Ionic Liquids

sample	ionic liquids	Zn(Ac) ₂ ·2H ₂ O/NaOH (mmol)	temperature (°C)	morphology	average diameter (nm)	length (nm)
1	[EMIM][BF ₄]	1:2	80	nanoparticles	10–20	
2	[EMIM][BF ₄]	1:4	80	nanorods	30–50	500–1500
3	[EMIM][BF ₄]	1:4	100	nanowires	30–40	1000–2000
4	[EMIM][BF ₄]	1:4	60	nanorods	50–80	500–800
5	[BMIM][BF ₄]	1:2	80	nanoparticles	30–40	
6	[BMIM][BF ₄]	1:4	80	nanorods	100–200	200–600
7	[BDiMIM][BF ₄]	1:2	80	nanoparticles	10–20	
8	[BDiMIM][BF ₄]	1:4	80	nanoparticles	20–50	
9	[BDiMIM][BF ₄]	1:4	60	nanoparticles	20–40	
10	[BDiMIM][BF ₄]	1:4	100	nanoparticles	40–60	

conditions were summarized in Table 1 (1-*n*-butyl-3-methylimidazolium tetrafluoroborate, abbreviated as [BMIM][BF₄], 1-*n*-butyl-2, 3-dimethylimidazolium tetrafluoroborate, abbreviated as [BDiMIM][BF₄], Scheme 1).

Photocatalytic Activity Experiments. The photocatalytic activity experiments on the obtained samples for the decomposition of Rhodamine B dyes in air were performed at room temperature. The obtained products of 20 mg were placed into a tubular quartz reactor of 100 mL 10⁻⁵ mol/L Rhodamine B aqueous solution. The reactor was surrounded with a UV lamp (125 W). The reaction mixture was stirred under UV irradiation. After the reaction, the mixture was sampled at different times and centrifuged for 5 min to discard any sediment. It was monitored through a wavelength scan on a UV-vis spectrophotometer. Then, absorption spectra were obtained.

Characterization. X-ray diffraction (XRD) patterns were carried out on a Rigaku D/max-2500 X-ray diffractometer equipped with graphite monochromatized Cu K α radiation ($\lambda = 0.154$ nm). The accelerating voltage was set at 50 kV, with a 100 mA flux at a scanning rate of 0.06°/s in the range of 10–60°. The transmission electron microscopy (TEM) images were taken on a Hitachi model H-800 instrument. High-resolution transmission electron microscopy (HRTEM) images and selected area electron diffraction (SAED) patterns were taken on a FEI TECNAI G² 20 S-TWIN microscope. The scanning electron microscopy images (SEM) were taken on a Hitachi S-3500N SEM. The X-ray photoelectron spectrum (XPS) was collected on a Kratos Axis Ultra DLD multitechnique X-ray photoelectron spectroscopy, using nonmonochromatized Mg K α X-ray as the excitation source. Energy-disperse X-ray analyses (EDXA) were performed on an EDX G2T20136–5 energy-disperse X-ray instrument. UV-vis absorption was monitored with a 721 UV-vis spectrophotometer. The room-temperature photoluminescence spectra were recorded on a SPEX FL 212 spectrometer with a xenon lamp. FTIR spectroscopy measurements were recorded with a Bruker Optics Instrument type Tensor 27 spectrophotometer. The surface area at the mesoscale was measured using a Quantachrome NOVA 4200e analyzer.

Results and Discussion

Structural Determination by X-ray Powder Diffraction. The XRD patterns of the samples prepared in three kinds of different ionic liquids are shown in Figure 1. Typical XRD patterns of nanostructures, including sample 2 (nanorods), sample 3 (nanowires), sample 5 (nanoparticles), sample 7 (nanoparticles), and sample 8 (nanoparticles) are shown in parts a–e of Figure 1, respectively. All of the diffraction peaks of the products can be indexed to the high crystalline wurtzite ZnO (hexagonal crystal system, $P6_3mc$ space group, JCPDS card No. 36–1451) with calculated lattice constants $a = 3.256$ Å and $c = 5.215$ Å (taken from sample 2 for example). No characteristic peaks are observed

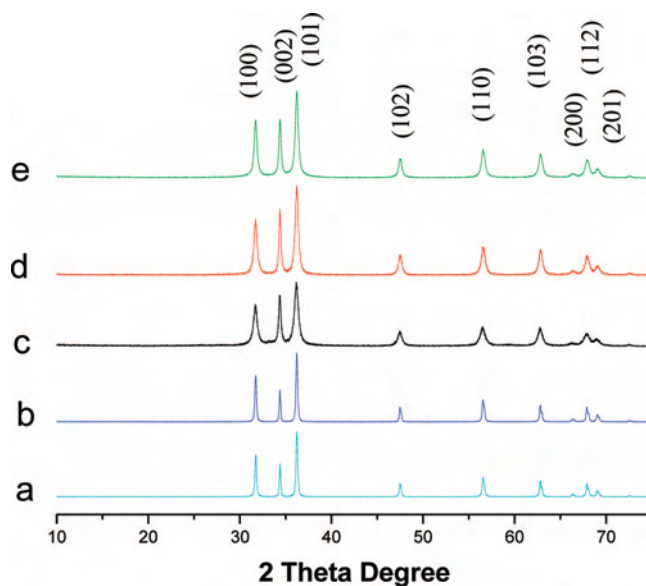


Figure 1. Powder XRD patterns of the typical products (a) sample 2, (b) sample 3, (c) sample 5, (d) sample 7, (e) sample 8.

for the other impurities such as Zn(OH)₂. Interestingly, compared with the XRD patterns of the ZnO nanoparticles (parts c–e of Figure 1), the intensity of the (002) peak in the patterns of 1D nanostructures, ZnO nanorods (part a of Figure 1), and nanowires (part b of Figure 1), is relatively weaker, similar to the diffraction patterns of the reported 1D ZnO nanostructures.¹⁵

Composition Analysis by XPS and EDXA. Further evidence for the quality and composition is obtained by XPS. Parts a and b of Figure 2 show the typical XPS spectra taken from the zinc and oxygen regions of the products (sample 3 for example). The binding energies obtained in the XPS analysis are corrected for specimen charging by referencing the C_{1s} to 285.2 eV. A strong peak at about 1021.9 eV can be attributed to Zn_{2p_{3/2}}. The peak profile for O_{1s} is asymmetric, the peak at about 530.2 eV can be indexed to the O(–2) in the ZnO, whereas the weaker shoulder peak at about 532.2 eV is due to chemisorbed oxygen caused by surface hydroxyl. The EDXA image (part c of Figure 2) also confirms that the components of the products are only zinc and oxygen. The copper signal is attributed to the copper meshes, whereas the carbon signal attributed to the membrane for HRTEM.

Morphologies of Samples 1–4. The morphologies of ZnO nanostructures prepared in ionic liquid [EMIM][BF₄] under different conditions are shown in Figure 3 and 4. Part a of

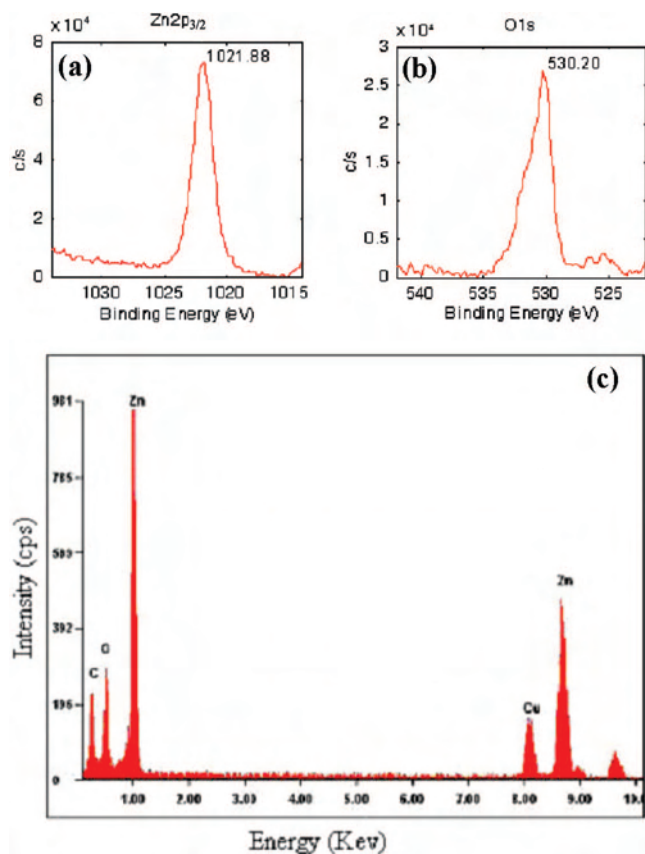


Figure 2. (a) XPS spectra of the sample 3, $Zn_{2p_{3/2}}$ region. (b) XPS spectra of the Sample 3, O_{1s} region. (c) EDXA spectrum of sample 3.

Figure 3 shows the TEM images of sample 1. The entire product is comprised of nanoparticles with an average diameter of about 10–20 nm, as can be seen from the size distribution histogram in the inset of part a of Figure 3, displaying irregular shapes. HRTEM images (part b of Figure 3) provide the structural detail of the ZnO nanoparticles, in which the interplanar spacings of the crystalline stripes is about 0.76 nm, which is about three times the separation of adjacent two (0002) lattice planes of reported hexagonal ZnO.⁹

The TEM image of sample 2 is shown in part c of Figure 3. The product is comprised of nanorods with an average diameter of about 30–50 nm and different lengths ranging from 500 to 1500 nm. The HRTEM image (part d of Figure 3) of sample 2 recorded from the edge of the nanorod shows that the interplanar spacing of the lattice stripes is about 0.25 nm, corresponding to the distance between adjacent two (0002) planes of hexagonal ZnO and indicates that the ZnO nanorods exhibit a preferred growth orientation along the [0001] crystal axis.⁹ The SAED pattern of the edge of the single nanorod indicates the single crystalline nature of the ZnO nanorods (inserted in part d of Figure 3).

Part e of Figure 3 shows the TEM images of sample 3. The entire product is comprised of large quantities of homogeneous 1D uniform ZnO nanowires with diameters of about 30–40 nm and lengths of up to 1–2 μm ; the size distribution histogram is shown in the inset of part e of Figure 3. The HRTEM image (part f of Figure 3) recorded from the single nanowire of sample 3 shows that the interplanar

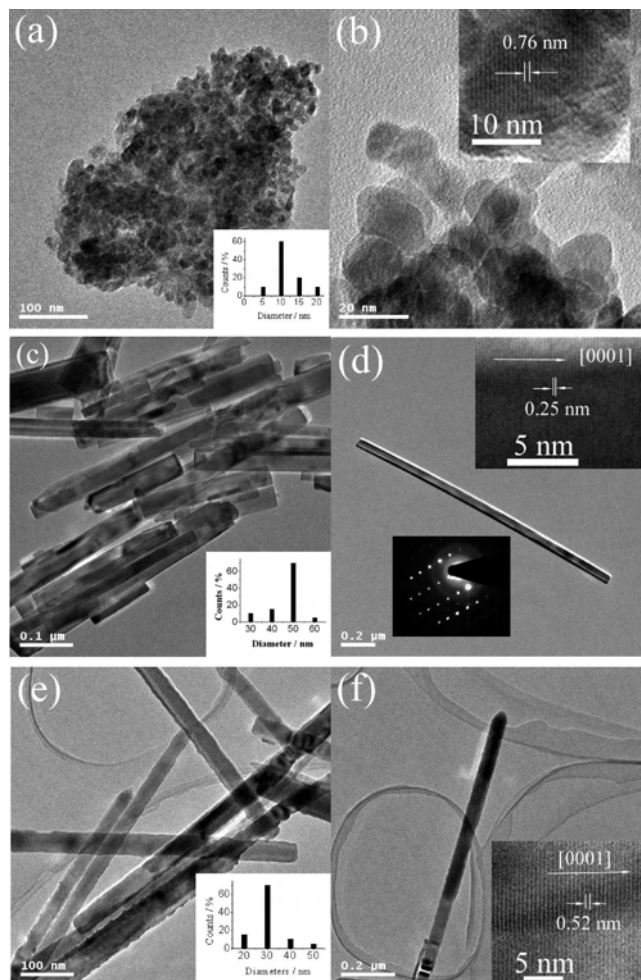


Figure 3. (a) TEM images of sample 1, (b) HRTEM image of sample 1, (c) TEM image of sample 2, (d) HRTEM image of sample 2, SAED patterns of sample 2 were inserted, (e) TEM image of sample 3, (f) HRTEM image of sample 3. (The insets in (a), (c), and (e) show the size distribution histogram).

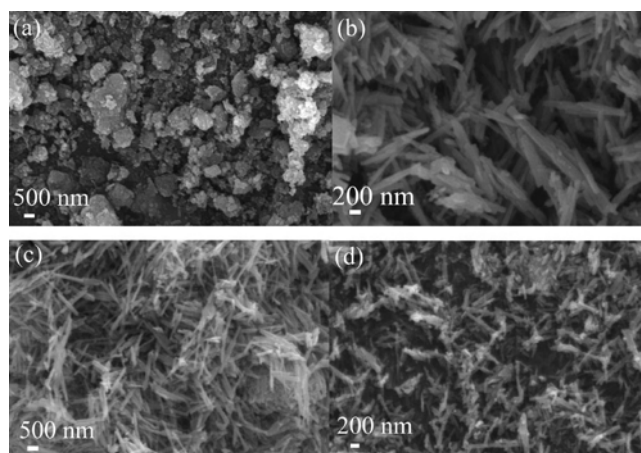


Figure 4. SEM images of the products (a) sample 1, (b) sample 2, (c) sample 3, and (d) sample 4.

spacing is about 0.52 nm, close to the separation between the adjacent two (0001) lattice planes of hexagonal ZnO, indicating that the ZnO nanowires exhibit a preferred growth orientation along the [0001] crystal axis.

The scanning electron microscopy (SEM) images, which could exhibit the common morphologies of samples 1–4 are

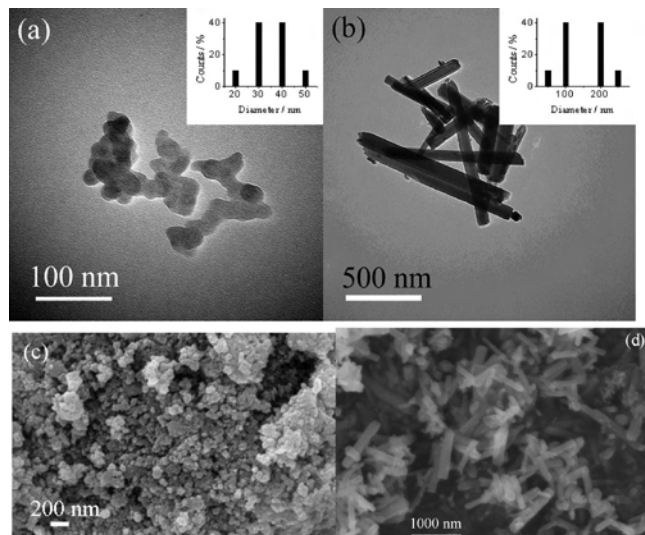


Figure 5. TEM images of (a) sample 5, (b) sample 6, and SEM images of (c) sample 5 and (d) sample 6. (The insets in (a) and (b) show the size distribution histogram).

shown in parts a–d respectively of Figure 4. Four samples have nanoparticles (part a of Figure 4), nanorods (part b of Figure 4), nanowires (part c of Figure 4), and incompletely developed nanorods (part d of Figure 4) morphologies, respectively. The observed results are consistent with those of TEM.

Morphologies of Samples 5–10. The TEM images of samples 5 and 6 prepared in the ionic liquid [BMIM][BF₄] are shown in parts a and b respectively of Figure 5. The SEM images of sample 5 and 6 are shown in parts c and d respectively of Figure 5. Sample 5 is composed of nanoparticles with an average diameter of about 30–40 nm, whereas sample 6 is comprised of short ZnO nanorods with diameters of about 100–200 nm and lengths up to 200–600 nm, as can be seen from the size distribution histogram in the inset of parts a and b of Figure 5.

The morphologies of ZnO nanostructures prepared in ionic liquid [BDiMIM][BF₄] are shown in Figures 6 and 7. Part a of Figure 6 shows the TEM images of sample 7. The product is composed of ZnO nanoparticles with average diameters of about 10–20 nm with the size distribution histogram, as shown in the inset. HRTEM images are studied to provide the structural details of sample 7, in which the interplanar spacings of the crystalline stripes (part b of Figure 6) are about 0.25 nm and can be indexed to the distance between the adjacent two (0002) planes of hexagonal ZnO. The TEM images of samples 9 and 10 are shown in parts c and d of Figure 6. Sample 9 is composed of ZnO nanoparticles with diameters of about 20–40 nm, and sample 10 is also composed of ZnO nanoparticles with diameters of about 40–60 nm. The SEM images of parts a–d of Figure 7 show the morphology of samples 7–10, respectively, indicating all of the samples with nanoparticles morphologies.

Effect of the Structure of Ionic Liquids on the Morphologies of ZnO. Samples 2, 6, and 8 were synthesized in three different ionic liquids mentioned above under the same other conditions (Table 1). By comparing the morphologies of three samples, we investigate the effect of the

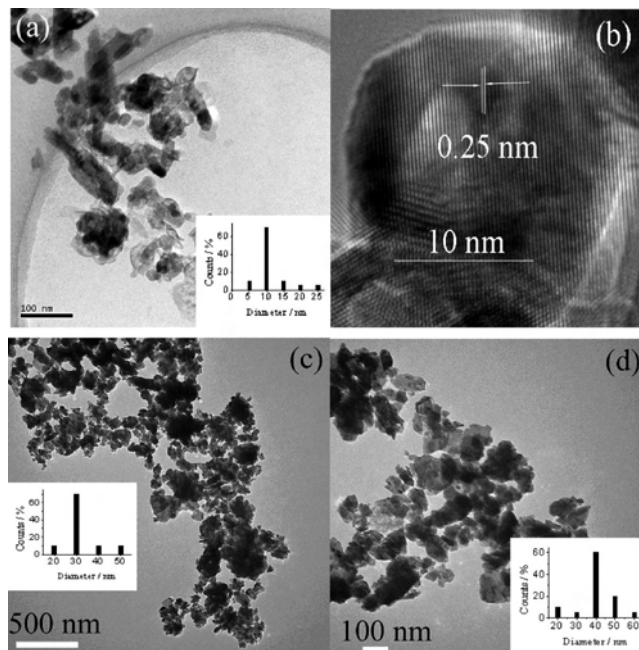


Figure 6. TEM (a) and HRTEM images (b) of sample 7, TEM images of sample 9 (c) and sample 10 (d). The insets in (a), (c), and (d) show the size distribution histogram.

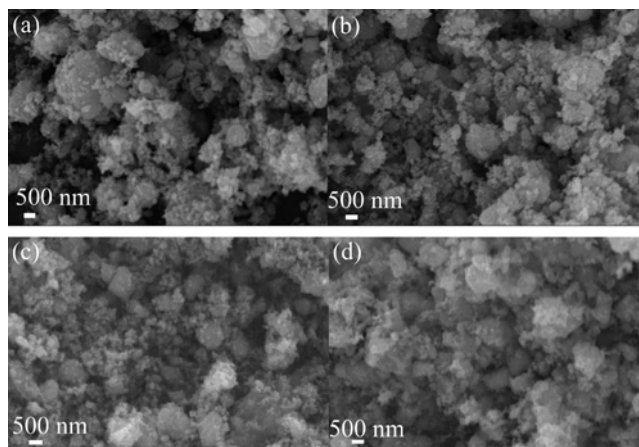
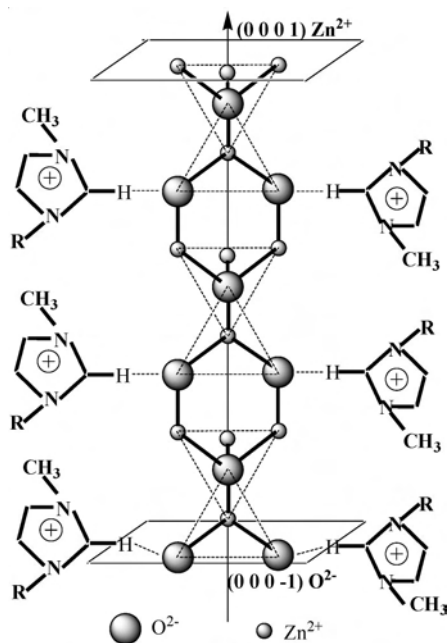


Figure 7. SEM images of (a) sample 7, (b) sample 8, (c) sample 9, (d) sample 10.

structure of ionic liquids on the morphologies of the final ZnO nanostructures. When ionic liquid [EMIM][BF₄] was introduced to the reaction system, ZnO nanorods with lengths of about 500–1500 nm are obtained (sample 2). If [BMIM][BF₄] was introduced to the reaction system with the same other reaction parameters, the morphologies exhibit significant difference. Although the products (sample 6) are still composed of ZnO nanorods, the length (200–600 nm) is much shorter than that of sample 2. This result indicates that the length of the chains at position 1 of imidazole ring of the ionic liquid affects the morphologies of the final products; longer chains will hinder the 1D ZnO nanostructures from growing longer because of the steric hindrance effect.

However, when ionic liquid [BDiMIM][BF₄] was introduced to the reaction system with the same other reaction parameters, the morphology of the products is completely different. The entire product (sample 8) is comprised of

Scheme 2. Growth Schematic Diagram of 1D ZnO Nanostructures in Ionic Liquid



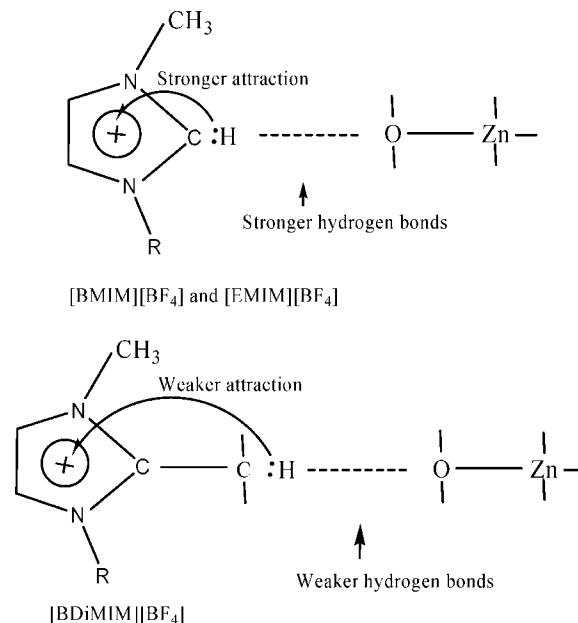
nanoparticles, no 1D ZnO nanostructures are obtained. The case indicates that the hydrogen atoms at position 2 of the imidazole ring perhaps are associated with the formation of preferential growth of the ZnO nanostructures.

To better understand the effect of ionic liquid on the ZnO nanostructures' growth, control experiments are done under the same reaction. By directly grinding $\text{Zn}(\text{CH}_3\text{COO})_2 \cdot 2\text{H}_2\text{O}$ and NaOH with the mole ratio as 1:4 in the absence of ionic liquid, irregular particles of ZnO are obtained, which suggests that ionic liquid in the reaction system plays an important role for the preferential growing of ZnO nanostructures.

Possible Formation Mechanism. Systematic investigations of the formation mechanism of ZnO nanostructures in different ionic liquids are important for the morphology control of ZnO products, which as of yet has not been reported in detail. It is well-known that the size of the products depends on the rate of nucleation and the growth rate of the product. We add the ionic liquid into the reaction system for two reasons: First, the ionic liquid in the synthetic process may serve as an agglomeration inhibitor, which can hinder the fast contact of particles of two substrates. The reaction process is slightly slow but still mild enough to let the molecule self-assemble, and the rate of nucleation is faster than the growth rate. Second, the special structure of the ionic liquid can induce the preferential growth of ZnO crystal nuclei in a certain direction, thus allowing the nanocrystals to undergo self-organization into the desired nanostructure, just as a soft template.

A growth schematic diagram of 1D ZnO nanostructures in ionic liquid is shown in Scheme 2. Structurally, the wurtzite-structured ZnO crystal is described as a number of alternating planes composed of 4-fold tetrahedrally coordinated O^{2-} and Zn^{2+} ions stacked alternatively along the c axis.^{18,35} Zinc and oxygen atoms are arranged alternatively along the c axis, thus the top surface is Zn^{2+} -terminated

Scheme 3. Schematic Illustration of the Comparison of Hydrogen Bonds in Ionic Liquids [EMIM][BF₄], [BMIM][BF₄], and [BDiMIM][BF₄]



(0001) and the bottom surface is O^{2-} -terminated (000-1).^{18,35} Besides these surfaces, ZnO has other typical side surface such as O^{2-} -terminated (10-11), (10-10). The cations of ionic liquid can be easily adsorbed on the surface of the O^{2-} -terminated surface by electrostatic force, and the hydrogen bond, formed between the hydrogen atom at position 2 of the imidazole ring and the oxygen atoms of $\text{O}-\text{Zn}$, may act as an effective bridge to connect the O^{2-} -terminated plane of the produced nuclei of metal oxide and cations of ionic liquids, thus resulting in a relatively slow growth rate for the O^{2-} -terminated surface in comparison to other crystal surfaces (Scheme 2). As a result, the preferential growth of Zn^{2+} -terminated (0001) face that originally has the highest growth rates¹⁹ is realized.

To demonstrate the hydrogen bonds formed between the ZnO nuclei and the ionic liquids, the FTIR spectra were performed, as shown in Figure S1 of the Supporting Information. FTIR spectra of pure [EMIM][BF₄] and [EMIM][BF₄]/ZnO nanorods are presented in parts a and b respectively of Figure S1, and the main adsorption peaks are listed in Table 1 of the Supporting Information. In part a of Figure S1, the bands at 3149 and 3094 cm^{-1} are assigned to the stretching vibration of C(2)-H in an imidazole ring. The adsorption bands at 1638, 1565, and 1459 cm^{-1} in pure [EMIM][BF₄] are due to the skeleton stretching vibration of the imidazole ring.^{34b} Compared with that of the pure [EMIM][BF₄], the FTIR spectrum of [EMIM][BF₄]/ZnO nanorods displayed significant differences. The adsorption band related to the stretching vibration of C(2)-H in imidazole ring is broadened and weakened after ZnO nanorods were obtained in ionic liquid [EMIM][BF₄], which demonstrates that there are strong interactions between ionic liquids and ZnO nanorods. The above changes of bands demonstrate the existence of hydrogen bonds between the hydrogen atom at position 2 of the imidazole ring and the

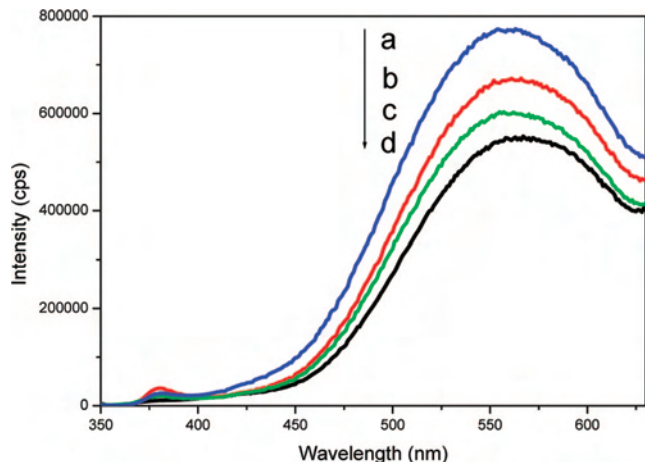


Figure 8. The room-temperature photoluminescence of the products (a) sample 1, (b) sample 3, (c) sample 2, and (d) sample 6.

oxygen atoms of O–Zn, which may play a crucial role in the preferential growth of 1D ZnO nanostructures.

The imidazole ring is an electron-withdrawing group and it can attract the electron pair shared by hydrogen and carbon of position 2 of imidazole ring, thus the hydrogen bonding between ionic liquids [EMIM][BF₄], [BMIM][BF₄], and ZnO crystal cores is strong (Scheme 3). But when ionic liquid [BMIM][BF₄] is replaced by [BDiMIM][BF₄], the hydrogen atoms at position 2 of the imidazole ring are replaced with a methyl group, the effect of hydrogen bonding is changed. As the attraction of the imidazole ring to electron-pair becomes weaker, hydrogen bonding is weaker (Scheme 3), the connection of [BDiMIM] cations and ZnO crystalline cores becomes rather loose, and ZnO crystal cores can grow relatively freely. As a result, only ZnO nanoparticles are formed.

Effect of the Amount of NaOH. The effect of NaOH on the morphology of the products in three ionic liquids is also investigated. In ionic liquid [EMIM][BF₄], ZnO nanoparticles and nanorods can be selectively prepared only by tuning the mole ratio of Zn(CH₃COO)₂·H₂O and NaOH from 1:2 (sample 1) to 1:4 (sample 2) under the same reaction. 1D ZnO nanostructures can only be obtained in the presence of excess NaOH, which is explained as follows: According to the Lewis' theory, NaOH is a strong proton acceptor, and perhaps has a strong trend to take away the hydrogen atoms at position 2 of the imidazole ring, as can be seen from the FTIR spectrum. The adsorption band related to the stretching vibration of C(2)–H in the imidazole ring is slightly weakened after NaOH was added in ionic liquid [EMIM][BF₄] (Figure S2 in the Supporting Information). As a result of this attraction, the presence of excessive NaOH caused the change of the interaction between ZnO surface and ionic liquids, that is to say, it weakened the interaction between hydrogen atoms and carbon atoms at position 2 of the imidazole ring. On the contrary, the hydrogen bond, formed between the hydrogen atom at position 2 of the imidazole ring and the oxygen atoms of O–Zn were enhanced, playing a crucial role in the preferential growth of 1D ZnO nanostructures.

The same rule is also observed in the synthesis of ZnO nanostructures in ionic liquid [BMIM][BF₄]. The morphology

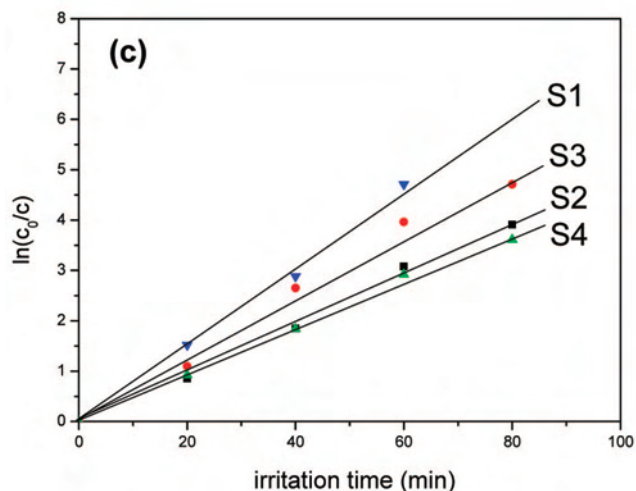
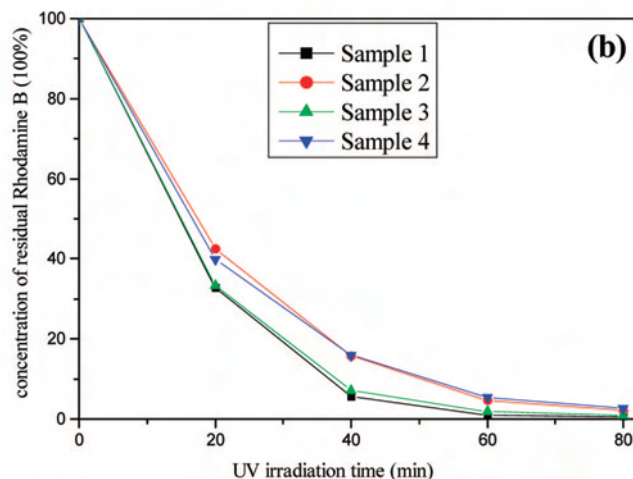
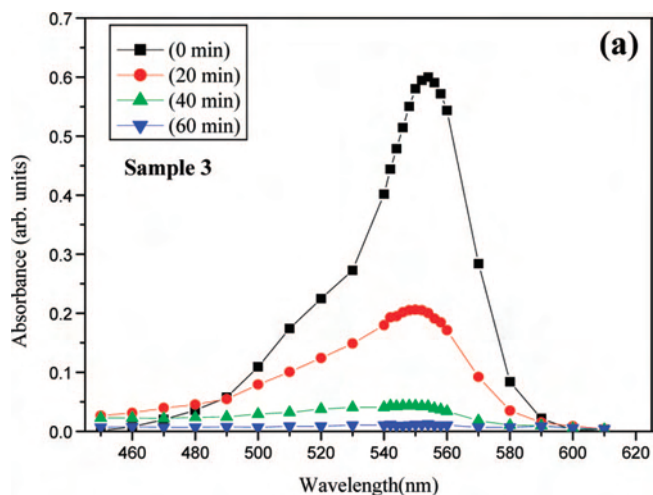


Figure 9. (a) Absorbance spectra of Rhodamine B dyes aqueous solutions after UV irradiation in the presence of sample 3 during different irradiation times, (b) the concentration of residual Rhodamine B with different UV irradiation times in the presence of samples 1–4, and (c) relative absorbance of Rhodamine B dyes in aqueous solutions after different UV irradiation times; S1 (blue): sample 1; S3 (red): sample 3; S2 (black): sample 2; S4 (green): sample 4.

of the products can be changed from nanoparticles (sample 5) to nanorods (sample 6) by changing the mole ratio of Zn(CH₃COO)₂·H₂O and NaOH from 1:2 to 1:4 under the same conditions.

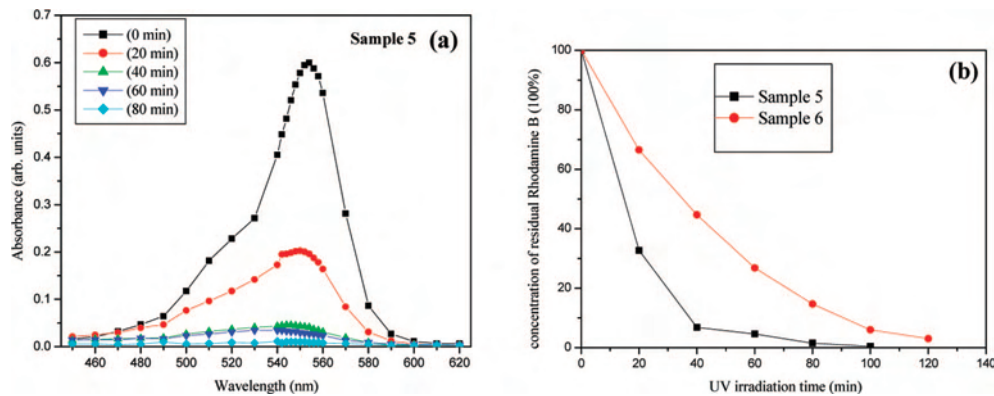


Figure 10. (a) Absorbance spectra of Rhodamine B dyes' aqueous solutions after UV irradiation in the presence of sample 5 during different irradiation times, and (b) the concentration of residual Rhodamine B with different UV irradiation times in the presence of samples 5–6.

However, in ionic liquid [BDiMIM][BF₄], the influence of the amount of NaOH is not so distinct. When we change the mole ratio of Zn(CH₃COO)₂·2H₂O and NaOH from 1:2 (sample 7) to 1:4 (sample 8) under the same conditions, the morphology is still similar to that of nanoparticles, only the diameters are slightly bigger. These results indicate that when ionic liquid [BDiMIM][BF₄] was introduced to the reaction system, the morphology of the as-obtained ZnO product may not be changed from nanoparticles to nanorods only by tuning the amount of NaOH.

Effect of the Temperature. The effect of the reaction temperature on the morphology of ZnO nanostructures is also investigated. In ionic liquid [EMIM][BF₄], when increasing the reaction temperature from 60 to 80 °C, the morphology of ZnO products evolves from incompletely developed ZnO nanorods (sample 4) to uniform ZnO nanorods (sample 2). When the reaction temperature is further enhanced to 100 °C, long and uniform ZnO nanowires (sample 3) are obtained. This result may be due to the fact that higher temperature may favor the growth of longer nanowires.

But the effect of temperature on the morphology of the nanostructures prepared in ionic liquid [BDiMIM][BF₄] is slight. Decreasing the reaction temperature from 80 °C (sample 8) to 60 °C (sample 9), the morphology is still similar to that of nanoparticles, and the diameters of sample 9 are little smaller than those of the sample 8. Increasing the reaction temperature to 100 °C, also, ZnO particles (sample 10) are obtained, only the diameters grow a little bigger, which indicates that elevation of temperature may favor the growth of larger ZnO nanoparticles. It is observed in our experiments that the morphology of the as-obtained ZnO product was always particle-like in shape when ionic liquid [BDiMIM][BF₄] was employed, and 1D ZnO nanostructures were not obtained by tuning the mole ratio of the reactants and reaction temperatures.

Luminescent Properties. The room-temperature photoluminescence spectra of the ZnO nanostructures with typical morphologies, such as ZnO nanoparticles (sample 1), ZnO nanorods (sample 2), ZnO nanowires (sample 3), and short nanorods (sample 6) are shown in Figure 8. The excited wavelength is 325 nm. Strong and broad green light emissions around 555 nm are observed in all of the samples, which come from the recombination of electrons in singly

occupied oxygen vacancies with photoexcited holes.²⁰ A very weak emission at 380 nm was observed in all of the samples, which comes from the recombination of excitonic centers.²¹ It is notable here that ZnO nanoparticles (sample 1) exhibit a stronger green emission than the ZnO nanowires (sample 3), the ZnO nanorods (sample 2), and the shorter ZnO nanorods (sample 6). It strongly indicates the existence of oxygen vacancies in the ZnO nanostructures. The smaller the grain size is and the long and thin the nanorods are, the stronger the intensity of the green luminescence is and the more the singly ionized oxygen vacancies are, which is consistent with the literature.²² This may be interpreted that the photoexcited holes in the small-sized ZnO nanocrystals and long 1D nanostructures have a better chance to find an oxygen defect.¹⁵

Photocatalytic Properties. The surface oxygen deficiencies of the as-obtained ZnO nanostructures make us think how to utilize this property. It was well reported that the high surface oxygen deficiencies may make some metal oxide such as TiO₂ and ZnO good photocatalysis for some organic compounds. The high surface oxygen deficiencies in oxide nanostructures are believed to be the electron capture center, which will reduce the recombination rate of electrons and holes.^{39,40} Recently, with the development of the textile industry, dye contamination is becoming a more serious environment problem. Within the overall category of dye-stuffs, Rhodamine B, one of the most important xanthene dyes, is widely used and has become a common organic pollutant.⁴¹ The photocatalytic activity experiments on the obtained 10 samples for the decomposition of Rhodamine B dyes in air are tested. To better understand the correlation between the size/shape and photocatalytic activity, the samples were divided into three groups according to different ionic liquids.

Photocatalytic Activity of Samples 1–4. Part a of Figure 9 shows the absorption spectra of photocatalytically degraded Rhodamine B aqueous solutions in the presence of sample 3 during different UV irradiation times. The residual concen-

(39) Xu, F.; Yuan, Z. Y.; Du, G. H.; Ren, T. Z.; Bouvy, C.; Halasa, M.; Su, B. L. *Nanotechnology* **2006**, *17*, 588.

(40) Yang, J. L.; An, S. J.; Park, W. I.; Yi, G. C.; Choi, W. Y. *Adv. Mater.* **2004**, *16*, 1661.

(41) Yu, D. Z.; Cai, R. X.; Liu, Z. H. *Spectrochim. Acta, Part A* **2004**, *60*, 1617.

tration of a Rhodamine B aqueous solution significantly decreased to 1.9% (0.19×10^{-6} mol/L) after 60 min of UV irradiation, then continued down to 0.9% (0.09×10^{-6} mol/L) of the initial concentration (10×10^{-6} mol/L) upon prolonging the irradiation time to 80 min. The residual concentration of the Rhodamine aqueous solution at 80 min UV irradiation in the presence of samples 1–4 is as follows (part b of Figure 9): Sample 1 (ZnO nanoparticles) (0.6%) < sample 3 (nanowires) (0.9%) < sample 2 (nanorods) (2%) < sample 4 (incompletely developed nanorods) (2.7%).

The kinetics of the photodegradation of Rhodamine B in the presence of samples 1–4 is also studied. The $\ln(C_0/C)$ of these samples is linear with the irradiation time (part c of Figure 9), which means that the photodegradation of Rhodamine B obeys the rules of a first-order kinetic reaction $\ln(C_0/C) = kt$. The apparent rate constants k of the photodegradation of Rhodamine B in the presence of samples 1, 3, 2, and 4 are 0.07205, 0.0614, 0.0491, and 0.0466/min, respectively; the larger the apparent rate constant k is, the higher the photocatalytic activity is.

Photocatalytic Activity of Samples 5–6. Part a of Figure 10 shows the absorption spectra of photocatalytically degraded Rhodamine B aqueous solutions in the presence of sample 5. The residual concentration of the Rhodamine aqueous solution could be significantly decreased to 4.6% (0.46×10^{-6} mol/L) after 60 min of UV irradiation and then down to 1.5% (0.15×10^{-6} mol/L) upon prolonging the irradiation time to 80 min, respectively. The residual concentration of a Rhodamine B aqueous solution at 80 min UV irradiation in the presence of samples 5 and 6 is as follows (part b of Figure 10): Sample 5 (ZnO nanoparticles) (1.5%) < sample 6 (short ZnO nanorods) (14.7%).

Photocatalytic Activity of Sample 7–10. During the degradation of Rhodamine B dyes over the sample 7 (part a of Figure 11), the residual concentration of Rhodamine aqueous solution significantly decreased to 2.1% (0.21×10^{-6} mol/L) after 60 min UV irradiation and then continued down to zero upon prolonging the irradiation time to 80 min. The further comparative experiments were carried out to study the relationship between the photocatalytic activity and morphology of the products (part b of Figure 11). The residual concentration of the Rhodamine B aqueous solution at 80 min of UV irradiation in the presence of samples 7–10 is as follows (part b of Figure 11): Sample 7 (0%) < sample 8 (0.5%) < sample 9 (1.3%) < sample 10 (3.2%).

Part c of Figure 11 shows the decomposition of the Rhodamine B aqueous solution at 80 min of UV irradiation in the presence of samples 1–10 ($(C_0 - C)/C_0 \times 100\%$), which follows this sequence: Sample 7 (100%) > sample 8 (99.5%) > sample 1 (99.4%) > sample 3 (99.1%) > sample 9 (98.7%) > sample 5 (98.5%) > sample 2 (98.0%) > sample 4 (97.3%) > sample 10 (96.8%) > sample 6 (85.3%). By comparing the relationship between the photocatalytic activity results and the morphologies of the products, it could be found that the uniform grain size of ZnO nanoparticles, homogeneous long and thin 1D ZnO nanostructures exhibit high photocatalytic activity on the Rhodamine B dyes.

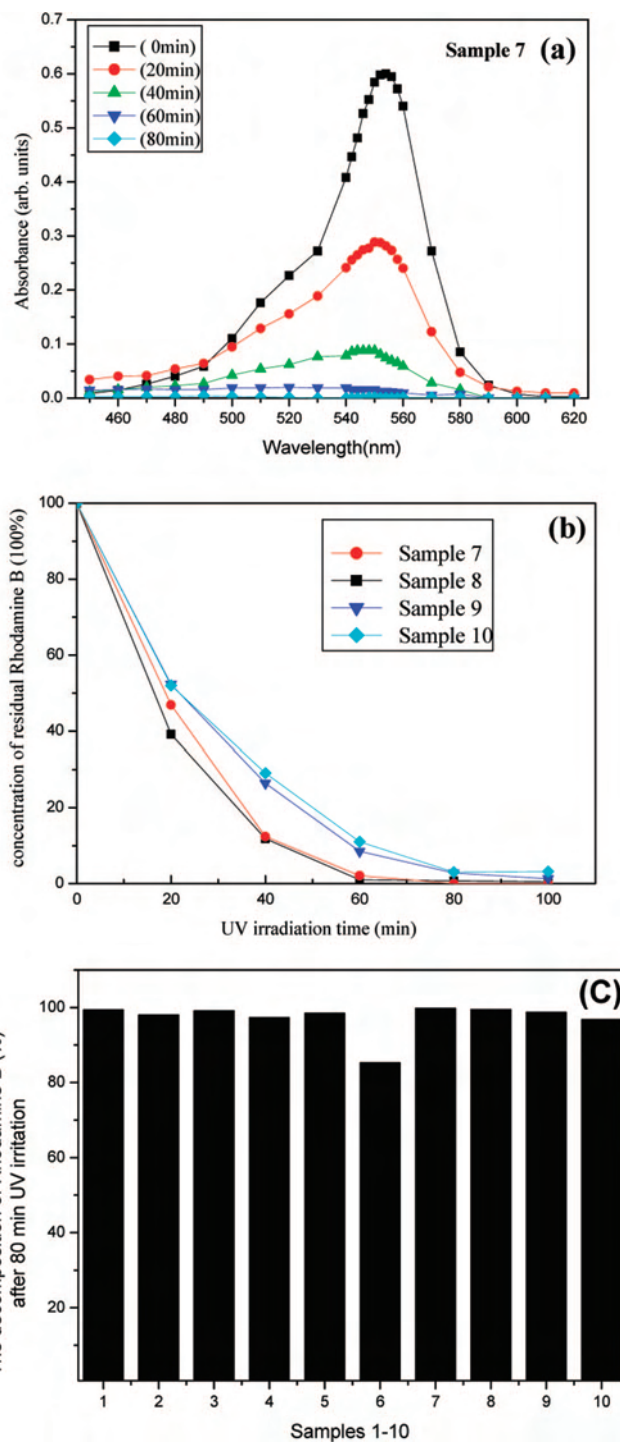


Figure 11. (a) Absorbance spectra of Rhodamine B dyes' aqueous solutions after UV irradiation in the presence of sample 7 during different irradiation times, (b) the concentration of residual Rhodamine B with different UV irradiation times over the as-obtained samples 7–10, and (c) the residual concentration of Rhodamine B in aqueous solution at 80 min UV irradiation in the presence of samples 1–10.

Photodegradation Mechanism. The photodegradation mechanism may be understood that, upon excitation, a conduction-band electron and a valence-band hole separate. The holes attack the surface hydroxyls and yield surface-bound hydroxy radicals. The surface $\cdot\text{OH}$ radicals can act as effective centers for photocatalytic reactions. Organic compounds, such as Rhodamine B, are believed to be destroyed through direct oxidation by the $\cdot\text{OH}$ radicals.⁴¹

Why do uniform ZnO nanoparticles and homogeneous long and thin 1D ZnO nanostructures show high photocatalysis activity in the photodegradation of the dyes of Rhodamine B? First, as observed in the TEM images of part a of Figure 3, part a of Figure 5, part a of Figure 6, part b of Figure 7, and part c of Figure 6. Samples 1, 5, 7, 8, and 9 are well-dispersed nanoparticles with average diameters of 10, 10, 20, 30, and 40 nm, respectively, which can be seen from the size distribution histogram in the inset of the TEM images. The homogeneous and small-sized ZnO nanostructures with effective high surface area are effective substrates for the adsorption of UV light and photocatalytic decomposition of dyes of Rhodamine B (sample 7 ($S_{\text{BET}} = 35.237 \text{ m}^2/\text{g}$) and Sample 1 ($S_{\text{BET}} = 34.651 \text{ m}^2/\text{g}$) for example). The smaller diameters are and the higher BET surface area is, the better photocatalysis activity is. Second, more intrinsic defects located at the surface of ZnO nanoparticles which are the electron capture center, will reduce the recombination rate of electrons and holes from the results of photoluminescence (Figure 8). Both of them would efficiently enhance the photocatalytic activity of the small sized ZnO nanoparticles.^{40,42} Similarly, samples 2 ($S_{\text{BET}} = 31.118 \text{ m}^2/\text{g}$) and 3 ($S_{\text{BET}} = 33.325 \text{ m}^2/\text{g}$), well-dispersed nanorods and nanowires, also show high photocatalytic activity because of the same reasons. The photocatalytic activity is not only related to the shape and size of the products but also to the degree of dispersion and homogeneity of the products. Sample 6 shows low photocatalytic activity because there is lower surface area ($S_{\text{BET}} = 21.764 \text{ m}^2/\text{g}$) in aggregated inhomogeneous short nanorods with an average diameter of 100–200 nm, as can be seen from the size distribution histogram in the inset of part b of Figure 5.

Interestingly, there is a correlation between the green luminescent intensity and photocatalytic activity; the stronger the intensity of the green luminescence is, the better photocatalytic activity of the obtained ZnO nanostructures on Rhodamine B is, which indicates more surface oxygen deficiencies in the ZnO nanostructures.

Conclusions

Low-dimensional ZnO nanostructures from nanoparticles to nanorods to nanowires are successfully synthesized in ionic

liquid at low temperature. The structures of the ionic liquids are found to be crucial to the morphologies of the final products. The hydrogen bonds formed between the hydrogen atom at position 2 of the imidazole ring and the oxygen atoms of O–Zn play a key role in the preferential growth of 1D ZnO nanostructures. The length of the alkyl chains at position 1 of the imidazole ring of the ionic liquid affects the morphologies of the final products. Room-temperature photoluminescent results reveal that the as-obtained ZnO nanostructures exhibit unique green emission property. Interestingly, the as-obtained ZnO nanostructures in different ionic liquids show strong size/shape dependence of photocatalysis activity. The ZnO nanostructures constructed in different ionic liquids were expected to be multifunctional materials for light emissions, electronic devices, and environment application, and the present work would give some inspirations to the controllable synthesis of other nanostructures in ionic liquids.

A series of shape-controllable ZnO nanostructures were synthesized in ionic liquids by the one-step low-temperature route, and systematical investigations were carried out for the effect of the cations of ionic liquids on the shape of ZnO nanostructures, and the forming mechanism of ZnO nanostructures in ionic liquids, as well as luminescent property and photocatalytic activity for the degradation of Rhodamine B. The results show that hydrogen bonds may play a crucial role for the directional growth of the 1D nanocrystals, and the well-dispersed homogeneous ZnO nanoparticles and nanowires display high photocatalytic activity for the degradation of Rhodamine B.

Acknowledgment. This work is supported by the National Natural Science Foundation of China (grants 20273033 and 20571044), FANEDD (grant 200732), 973 Program (grant 2005CB623607), and the Doctoral Start-up Fund of Xinjiang Normal University.

Supporting Information Available: FTIR spectra and frequencies of FTIR absorption bands. This material is available free of charge via the Internet at <http://pubs.acs.org>.

IC701094A

(42) Gao, X. D.; Li, X. M.; Yu, W. D. *J. Phys. Chem. B* **2005**, *109*, 1155.